Propagation and Development of Nonlinear Long Waves in a Water Saving Basin

Xueyi Li(✉), Feidong Zheng, Duoyin Wang, and Ming Chen

College of River and Ocean Engineering, Chongqing Jiaotong University, Chongqing, China
{xy_lee, wdy}@cqjtu.edu.cn

Abstract. The water saving lock layout plays a key role in addressing the navigation hydraulic problems with high dams. However, the study of the propagation and development of nonlinear long waves induced by ship-lock operation in a water saving basin has received less attention so far. Specially, the mechanisms governing the formation of secondary waves and the impact of these waves on the impoundments of the basin are still not fully understood. In the present study the entire evolution of a nonlinear long wave in a water saving basin was numerically simulated. The wave shape, wave celerity and wave force were analyzed. It was found that the leading edge of a long wave propagated along the water saving basin with a celerity which varied with time and space. Two distinct stages could be recognized and defined: a rapid acceleration phase characterized by a sharp increase in the celerity with propagation distance and a gentle acceleration phase where the long wave propagated in a more gradual manner. Moreover, the water surface slop of a long wave front equal to 0.045 could be used as an estimate of the occurrence of secondary waves. Furthermore, the present results highlighted the wave force on the impoundments of a water saving basin was controlled by wave nonlinearity. These results may provide theoretical guidance and technical support for the hydraulic design and operation of water saving locks.

Keywords: Water saving lock · Nonlinear long waves · Secondary waves · Wave reflection · Wave dispersion

1 Introduction

Separated and integrated water saving basins are two typical layouts for water saving locks. A flexible water level division scheme is the main advantage of the former layout although it always needs a large usage of land. In contrast, a relatively small land area is needed in the integrated layout. However, the determination of water level division scheme is a rather complicated and must consider many factors, such as the fluctuations of upstream and downstream water level, the area ratio of water saving basins and lock chamber, the thickness of water saving basin floor, the minimum depth of water saving basin, and the minimum height of water saving basin.

In previous studies, the water levels at different locations in water saving basins were assumed to rise or drop in the same speed, thus the free surface was treated as a

Y. Li et al. (Eds.): PIANC 2022, LNCE 264, pp. 565–577, 2023.
https://doi.org/10.1007/978-981-19-6138-0_49

plane. In fact, the operation of lock chambers is associated with temporal changes in the discharge, which increases up to a maximum value and subsequently decreases proportionally to the difference in water elevation between the basin and the lock chamber. Therefore, the operation of lock chambers leads to the formation of a long wave with a single wave crest or trough in the basin (Maeck and Lorke 2014). During the wave propagation, the positive part of the wave can evolve into secondary surges due to the combined effects of wave nonlinearity and dispersion (Castro-Orgaz and Chanson 2020; Soares Frazao and Zech 2002; Treske 1994; Zheng et al. 2018). As the secondary waves are superimposed on the original change in water level, they thus give rise to far larger maximum water level elevations (Benet and Cunge 1971). This phenomenon must be taken into account for the determination of the thickness of water saving basin floor, the minimum depth of water saving basin, and the minimum height of water saving basin (Treske 1994). Moreover, these waves will impose large impact loads on structural components (Zheng and Li 2021). In this study, the propagation of long waves and secondary waves in saving basins induced by the emptying operation of lock chambers were numerically investigated. The present results have the potential to provide some guidance for the design of water saving basins in integrated lock layout.

2 Numerical Method

2.1 Modeling

Based on a certain project, the length and width of the water saving basin were 337.56 m and 30.4 m, respectively. A rectangular water inlet was arranged in the longitudinal center of the basin with a length of 13.5 m and width of 4.5 m. As the longitudinal scale of the basin was much larger than the transverse scale, the basin was simplified as a two-dimension model in the vertical plane. Herein, only a half part of the basin was modeled by using a symmetric boundary. In the numerical model, the length and height of the basin were respectively 168.78 m and 6 m. The width and height of water inlet boundary were 1.78 m and 25 m, respectively.

After several mesh size distributions in the preliminary tests, the following grid scheme was used to achieve balance between the computing time and results quality. The maximum size of longitudinal x grid of water saving basin corridor is 0.02 m, and the maximum vertical grid is 0.02 m. The grid adopts quadrilateral grid, and the total number of grids is about 1.268 million, which is shown in the Fig. 1.

A specified mass inflow process is imposed at the bottom of the corridor, and the specific value is shown in the Fig. 2. The pressure inlet boundary condition P = Pa is adopted at the top of the basin. The symmetrical boundary is set at the symmetrical surface, and the remaining boundary is set as the wall. No-slip boundary conditions were applied to the walls in the simulation domain. The initial water depth in the water saving basin was selected on the basis of the actual engineering operation conditions, that is, $d_0 = 0.6$ m.

In conjunction with the renormalization group k–ε turbulence model, the numerical model solved the Reynolds-averaged Navier-Stokes (RANS) equations to predict the evolution of nonbreaking undular surges in a water–air system. The interface between

water and air was captured using the volume-of-fluid method. An explicit scheme and second-order upwind scheme were applied for time and spatial discretization, respectively. The SIMPLE algorithm was adopted for pressure and velocity coupling.

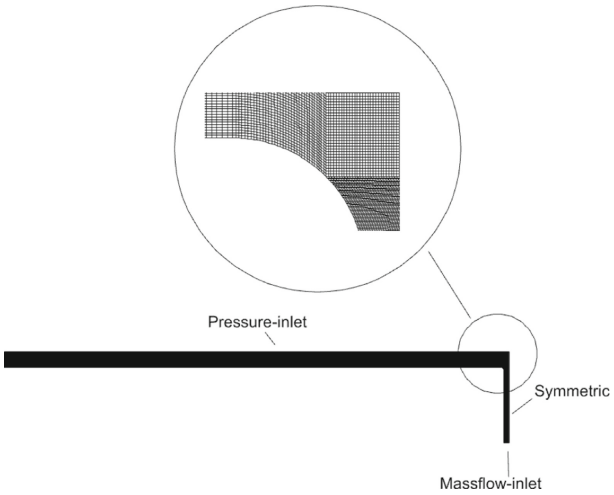

Fig. 1. Numerical model.

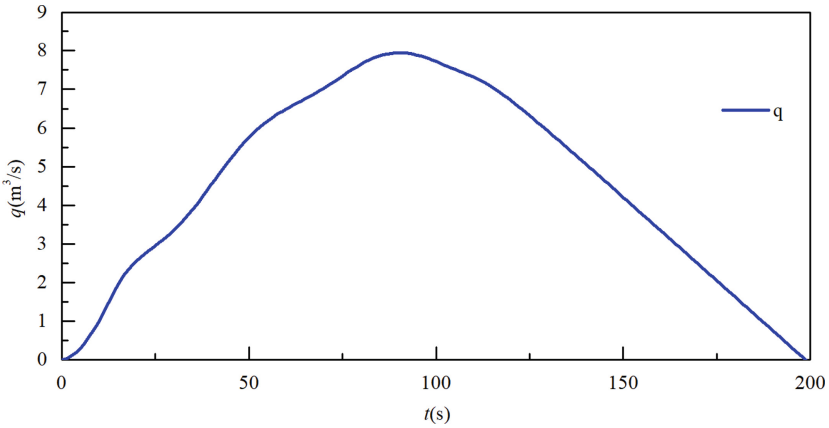

Fig. 2. Average discharge per unit width.

2.2 Validation

The formation of secondary waves is due to the continuous effect of wave nonlinearity in the long wave propagation, which leads to an enhanced water wave dispersion. Hence, the key to modelling secondary waves is therefore the ability of the numerical method used to effectively account for both wave nonlinearity and dispersion. Zheng and Li (2021) devised an experimental setup to validate a similar numerical model. Figure 3 provided a comparison between measured wave profiles and calculated results. Both the propagation of long waves and the evolution of secondary waves are well produced.

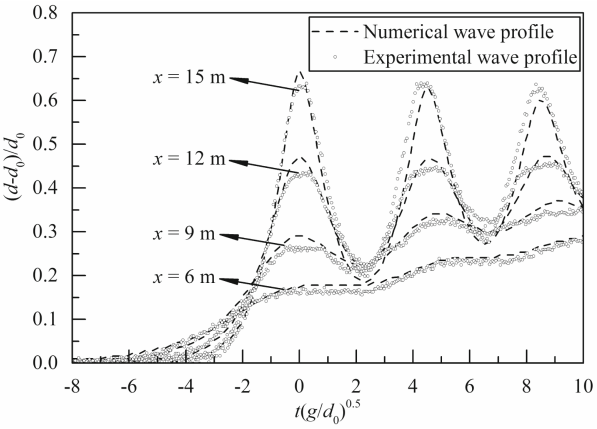

Fig. 3. Comparison the results of experimental and numerical

3 Results and Discussion

3.1 Wave Profile

The emptying of the lock chamber generated a nonlinear long wave comprising a positive wave and a subsequent negative wave in the water saving basin (Maeck and Lorke 2014). When the long wave advancing in still water, its positive part tended to steepen due to wave nonlinearity and subsequently disintegrated into a series of well formed free-surface undulations (Soares Frazao and Zech 2002). The propagation of the secondary wave was accompanied by a significant wave amplification (Zheng et al. 2021a). After that, the secondary wave transferred into a breaking regime (Pelinovsky et al. 2015). During the further propagation of the secondary wave, its free-surface undulations disappeared and the wave evolved into a breaking bore (Chanson

2010a, Koch and Chanson 2009). The long wave and secondary wave were subject to positive reflection at the upstream and downstream impoundments of the water saving basin, which resulted into increased wave heights (Zheng et al. 2021b). After the first wave reflection, these waves propagated either in the flow direct or against an unsteady flow in the impounded basin. It should be noted that in this process, the change of the secondary wave type occurred due to the combined effect of wave nonlinearity and dispersion. Therefore, in the subsequent analyses, the investigation on the free-surface characteristics was restricted to the wave propagation prior to the secondary wave reflection at the impoundment.

The wave profile evolution before wave reflection is presented in Fig. 4. At t = 5.17 s, the surface sarcomport appeared at the top of the inlet of the water saving basin. At t = 10.12 s, the surface sarcomport region extended. At t = 15.1 s, a nonlinear long wave propagated to the left impoundment with the maximum water surface slope of the wave front of 0.022. At t = 20.11 s, the maximum slope of water surface slope reached 0.045. At t = 25.1 s, a series of well-formed undulations appeared at the wave front of the long wave. At t = 30.11–35.1, the propagation of the secondary wave was characterized by a considerable wave amplifications. At t = 45.2–55.2 s, the secondary wave showed some wave breaking and eventually evolved into a breaking bore. At this moment, the wave front of the long wave was characterized by a steep water wall. At t = 60.2s, the wave front arrived at the upstream impoundment.

Figure 5 exhibits the development of wave profiles after the first wave reflection. The secondary wave located at the wave front of the long wave showed an undular appearance immediately after wave reflection. At t = 95.2 s, the secondary wave exhibited some wave breaking immediately after its wave amplitude reached the maximum value. At t = 115.2 s, the free-surface undulations disappeared. The wave profiles after the long wave arrived at the downstream symmetrical boundary are presented in Fig. 6. Notably, the collisions of long waves facilitated the occurrence of undular secondary waves. In this context, the wave length of the secondary wave increased and the slope of the wave front decreased. The evolution of these waves after the second wall reflection is presented in Fig. 7. It can be seen that the wave amplitude of the secondary wave during wave propagation showed obvious wave attenuation due to the combined effect of wall friction and dispersion (Chanson 2010b).

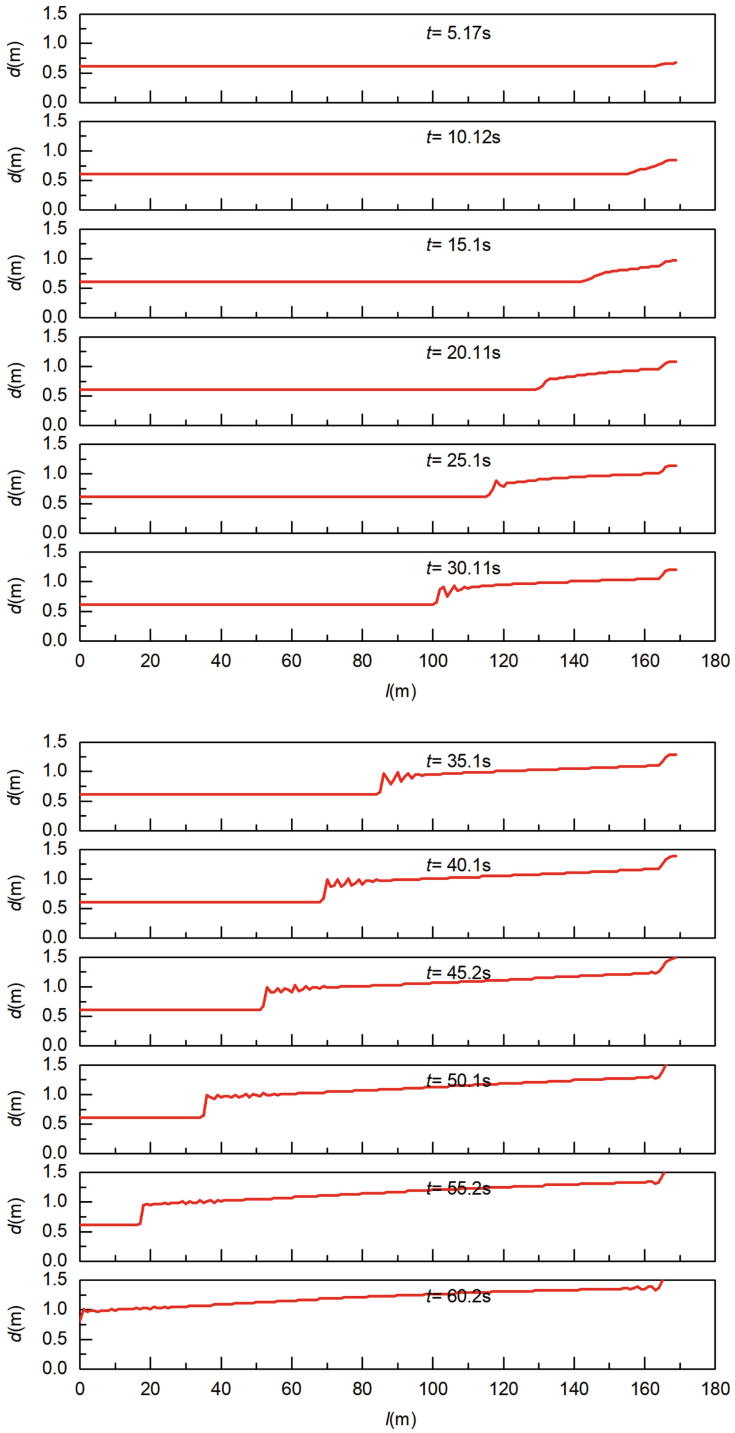

Fig. 4. Wave profile evolution before wall reflection.

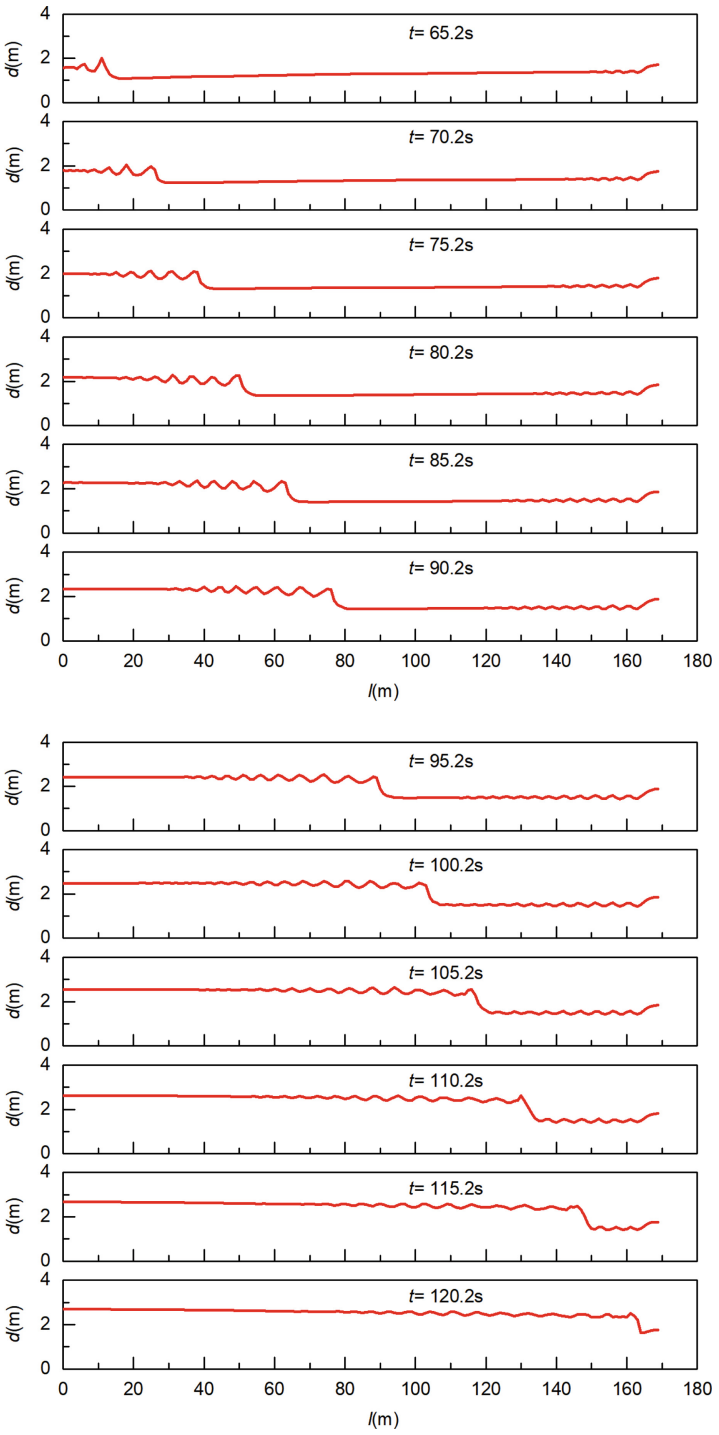

Fig. 5. Wave profile evolution after the first wall reflection.

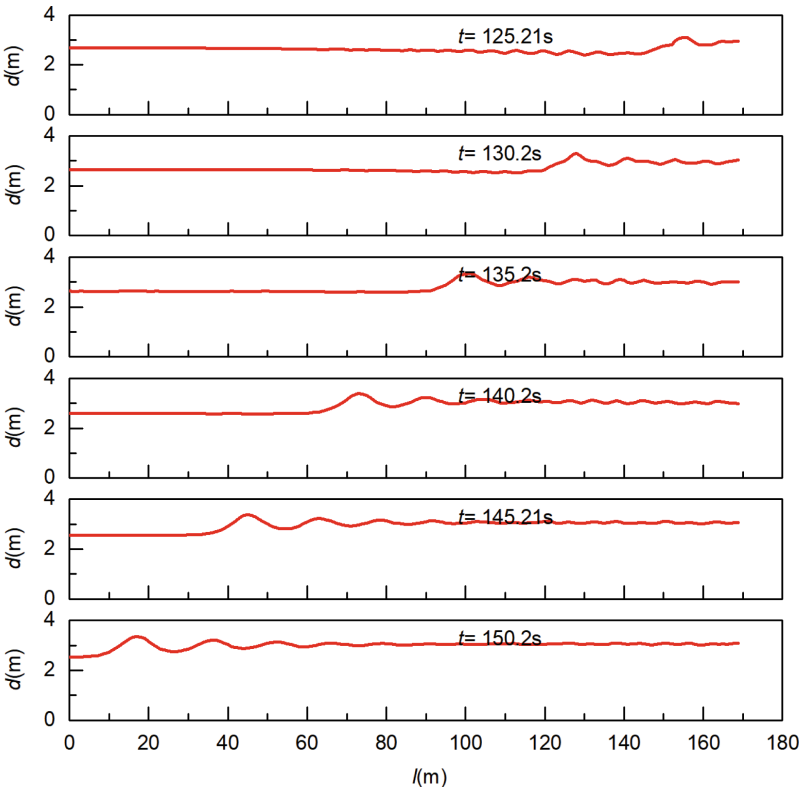

Fig. 6. Wave profile evolution after wave collision.

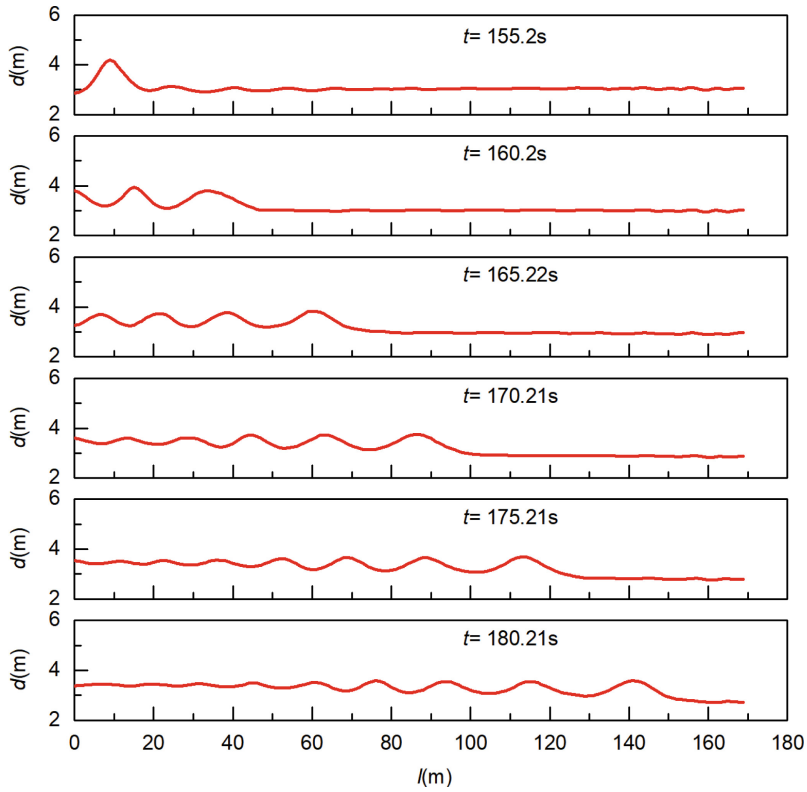

Fig. 7. Wave profile evolution after the second wall reflection.

3.2 Wave Celerity

The leading edge of a long wave propagated along the water saving basin with a celerity which varied with time and space. The evolution of long wave celerity in the water saving basin is shown in Fig. 8. C1 referred to the wave celerity of the long wave propagating in still water. C2 denoted the wave celerity of the long wave propagating from the upstream impoundment to the symmetric boundary immediately after the first wall reflection. C3 was the wave celerity of the long wave advancing from the symmetric boundary to the upstream impoundment. C4 was defined as the wave celerity after the second wall reflection. It can be observed that two distinct phases existed in the propagation process of the long wave in still water: a rapid acceleration phase characterized by a sharp increase in the celerity with propagation distance up to x = 16.78 m, and a gentle acceleration phase where the long wave propagated in a more gradual manner with a maximum wave celerity equal to 3.5 m/s. It is worth noting that the wave celerity at the phase transition was 2.5 m/s, which was close to the shallow wave celerity (i.e., 2.4 m/s). A sharp drop in the wave celerity was observed shortly immediately after the first wall reflection, i.e., C2 = 2.6. After that, the wave celerity showed some fluctuations during the subsequent wave propagation. C3 and C4

exhibited some irregular fluctuations over propagation distance with average values of 5.6 m/s and 5.2 m/s, respectively.

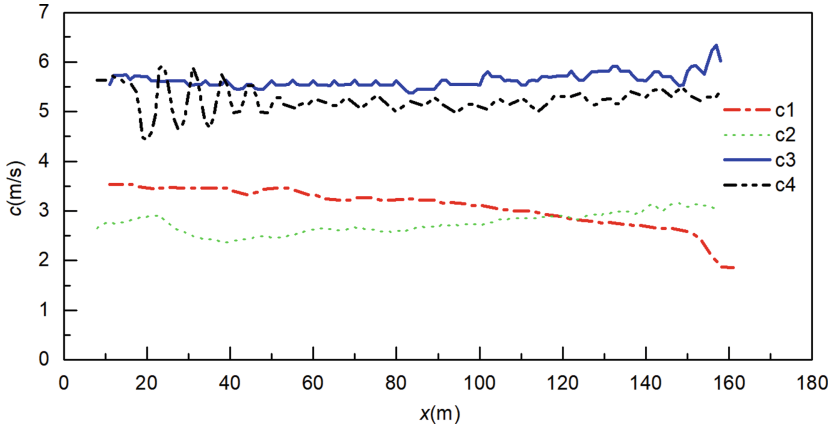

Fig. 8. Wave celerity evolution during wave propagation.

3.3 Wave Force

The temporary evolution of wall force at the upstream impoundment is present in Fig. 9. Considering the first wall reflection, the wave force profile exhibited a double maximum structure due to the nonhydrostatic effects resulted from wave nonlinearity (Cooker et al. 1997). The wall force increased significantly with the water level and reached the first maximum value before the maximum wave run up at the impoundment. Subsequently, the force profile presented a local minimum value near the maximum wave run up and the second maximum value. For the second wall reflection, the wall force tended to oscillated in phase with the free-surface undulations. In this situation, the wave nonlinearity was rather weak and only single peak in force distribution was exhibited (Chen et al. 2015).

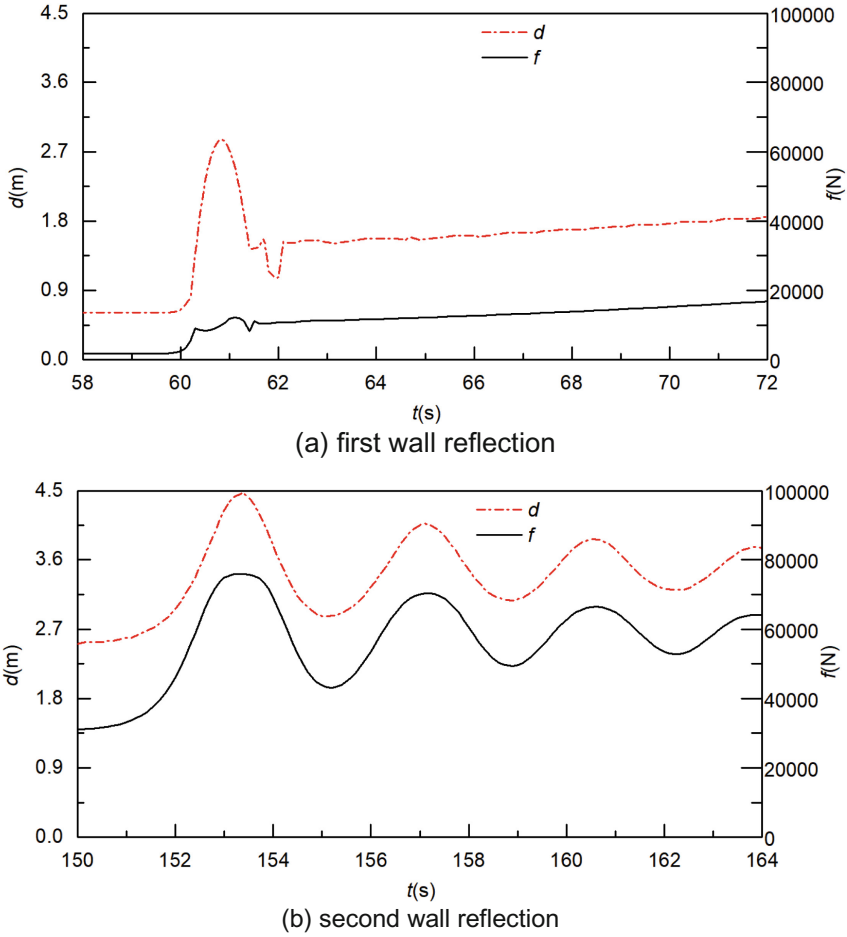

Fig. 9. Time evolution of free surface and wall force.

4 Conclusions

The basin in a water saving lock is an impounded channel where long waves generated by the filling and emptying operation of lock chambers exist. During the propagation of the waves along the basin, several complicated hydraulic phenomena can be observed, such as the appearance of secondary waves over the body of the long waves, the wave type transition of secondary waves, and the wave reflection at the upstream and downstream impoundments. In this study, the propagation and evolution of long waves induced by ship-lock operation in a water saving basin was numerically investigated. The results showed the leading edge of a long wave propagated along the water saving

basin with a celerity which varied with time and space. Two distinct stages were observed in the propagation process of the long wave in still water: a rapid acceleration phase characterized by a sharp increase in the celerity with propagation distance up to 16.78 m, and a gentle acceleration phase where the long wave propagated in a more gradual manner. It was found secondary waves occurred on the wave front of the long wave when its slop exceeded 0.045. In addition, the present results demonstrated that the impact of water waves in a water saving basin on impoundments was strongly dependent on wave nonlinearity. The present results have the potential to provide some guidance for the optimum design of water saving basins in integrated lock layout.

Acknowledgements. This study was supported by the China Postdoctoral Fund (Grant No. 2021M700620); Natural Science Foundation of Chongqing, China (Grant No. cstc2021jcyj-bshX0049; cstc2020jcyj-bshX0043); Natural Science Funds of Chongqing (No. cstc2019jcyj-msxmX0759).

References

Benet F, Cunge JA (1971) Analysis of experiments on secondary undulations caused by surge waves in trapezoidal channels. J Hydraul Res 9(1):11–33

Castro-Orgaz O, Chanson H (2020) Undular and broken surges in dam-break fows: a review of wave breaking strategies in a Boussinesq-type framework. Environ Fluid Mech 20(6):1383–1416

Chanson H (2010) Undular tidal bores: basic theory and free-surface characteristics. J Hydraul Eng 136(11):940–944

Chanson H (2010) Unsteady turbulence in tidal bores: Effects of bed roughness. J Waterw Port Coast Ocean Eng 136(5):247–256

Chen YY, Kharif C, Yang JH, Hsu HC, Touboul J, Chambarel J (2015) An experimental study of steep solitary wave reflection at a vertical wall. Eur J Mech - B/Fluids 49:20–28. https://doi.org/10.1016/j.euromechflu.2014.07.003

Cooker MJ, Weidman PD, Bale DS (1997) Reflection of a high-amplitude solitary wave at a vertical wall. J Fluid Mech 342:141–158

Koch C, Chanson H (2009) Turbulence measurements in positive surges and bores. J Hydraul Res 47(1):29–40

Maeck A, Lorke A (2014) Ship-lock induced surges in an impounded river and their impact on subdaily flow velocity variation. River Res Appl 30(4):494–507

Pelinovsky EN, Shurgalina EG, Rodin AA (2015) Criteria for the transition from a breaking bore to an undular bore. Izv Atmos Ocean Phys 51(5):530–533. https://doi.org/10.1134/S0001433815050096

Soares Frazao S, Zech Y (2002) Undular bores and secondary waves - experiments and hybrid finite-volume modelling. J Hydraul Res 40(1):33–43

Treske A (1994) Undular bores (Favre-waves) in open channels—Experimental studies. J Hydraul Res 32(3):355–370

Zheng F, Li Y, Xuan G, Li Z, Zhu L (2018) Characteristics of positive surges in a rectangular channel. Water 10(10):1473

Zheng F, Wang P, An J, Li Y (2021) Characteristics of undular surges propagating in still water. KSCE J Civ Eng 25(9):3359–3368. https://doi.org/10.1007/s12205-021-0858-3

Zheng F, Wang P, Wang M, Zhang J (2021) The evolution and runup of nonbreaking undular surges. Mar Georesour Geotechnol 40(7):774–781
Zheng F, Li X (2021) Undular surges interaction with a vertical wall. Mar Georesour Geotechnol